

Voltage-driven dynamics of φ_0 -S/F/S Josephson junctions chains

G. A. Bobkov,¹ A. M. Bobkov,¹ and I.V. Bobkova^{1,2}

¹*Moscow Institute of Physics and Technology, Dolgoprudny, 141700 Moscow region, Russia*

²*National Research University Higher School of Economics, 101000 Moscow, Russia*

Superconductor/ferromagnet/superconductor Josephson junctions with anomalous phase shift φ_0 (φ_0 -S/F/S JJs) realize a coupling between the superconducting phase and the spin degrees of freedom. Consequently, the anomalous phase shift is a hallmark effect of superconducting spintronics and opens great perspectives for applications of such structures for controlling magnetization. Besides controlling the magnetization of a single ferromagnet, the direct coupling between the phase and the magnetization provides a possibility to establish and control a collective behavior of magnetic moments of different weak links in coupled chains of φ_0 -S/F/S JJs. Here we investigate voltage-driven dynamics of such chains and predict that the spin-phase coupling makes the conventional voltage-driven regime unstable. As a result the system undergoes a transition to other dynamical regimes, where clear signatures of the spin-phase coupling and the collective behavior are observed.

I. INTRODUCTION

Superconductivity is a macroscopic quantum state characterized as a whole by a superconducting phase. A basic property of superconducting systems is that the charge current and the superconducting phase are directly connected. A canonical example of such a relationship is a current-phase relationship (CPR) of a Josephson junction (JJ) [1]. The minimal form of the CPR is given by $j(\varphi) = j_c \sin \varphi$. Here $|j_c|$ is the critical current and φ is the phase difference between superconducting electrodes. The ordinary Josephson junctions have $j_c > 0$ yielding the zero phase difference ground state $\varphi = 0$. In certain cases $j_c < 0$ leading to the ground state $\varphi = \pi$. Such π -junctions have been realized in many systems, including S/F/S JJs [2–6], non-equilibrium S/N/S JJs [7, 8] and many other [9–12]. They can be used in superconducting logic and quantum computers[13–15].

Under the simultaneous breaking of time-reversal and inversion symmetries even more exciting situation can be realized in JJs. The CPR can take the form $j(\varphi) = j_c \sin(\varphi + \varphi_0)$ with the anomalous (spontaneous) ground state phase shift $\varphi_0 \neq 0, \pi$ [16, 17]. Such JJs have already been realized experimentally in systems with spin-orbit coupling, which is a manifestation of the inversion symmetry breaking, under the action of the applied magnetic field, which breaks the time-reversal symmetry.[18–21]

Another possibility to break the time-reversal symmetry is to use JJs via ferromagnetic interlayers (S/F/S JJs). It is more exciting because the anomalous ground state phase shift φ_0 depends on the direction of the interlayer magnetization and thus provides a direct magnetoelectric coupling between the magnetization and the superconducting phase. Therefore, φ_0 -S/F/S JJs realize not only a canonical coupling between the electric current and the phase, but also a coupling between the phase and the spin degrees of freedom. Consequently, the anomalous phase shift is a hallmark effect of superconducting spintronics[22, 23] and opens great perspectives for applications of such structures for controlling magnetization [16, 24–29]. To realize this coupling one can use for the

interlayers 2D or quasi 2D ferromagnets [30–32], where the Rashba spin-orbit coupling can be strong due to the structural inversion symmetry breaking. The other way is to exploit ferromagnetic insulator/3D topological insulator hybrids as interlayers [33–40].

Recently it was predicted that, besides controlling the magnetization of a single ferromagnet, which is a weak link of the φ_0 -S/F/S JJ, the direct coupling between the phase and the magnetization provides a possibility to establish and control a collective behavior of magnetic moments of different weak links in chains of φ_0 -S/F/S JJs [41–43]. The collective effects occur due to the extremely long-range interaction between the magnetic moments mediated by the macroscopic superconducting phase [41].

Here we investigate the behavior of such coupled chains of φ_0 -S/F/S JJs under the applied external dc voltage V and demonstrate that the presence of the coupling between the phase and the magnetic moment makes the conventional regime, which is usually realized in the coupled chains of JJs, unstable. The ac electric current induced by the applied voltage excites collective magnetic oscillations in such a system. Due to the magnetoelectric coupling they cause a back action on the superconducting phase, which can result in the development of instability. The instability begins to increase at voltages that exceed an eigenfrequency of the system [42] and the chain goes into another stable regime, in which the superconducting phase differences at individual JJs are not linear functions of time. This is accompanied by a significant freezing of the amplitude of oscillations of the magnetic moments and electric current in the chain. In addition the oscillation frequency of the current and the magnetic precession becomes a multiple integer of the Josephson frequency. Moreover, there is another stable dynamical regime, which is characterized by beats in the Josephson current with a period that corresponds to the difference in frequencies between the acoustic and optical modes of the collective oscillations of the chain [42]. This regime is clearly seen at the IV-characteristic of the chain.

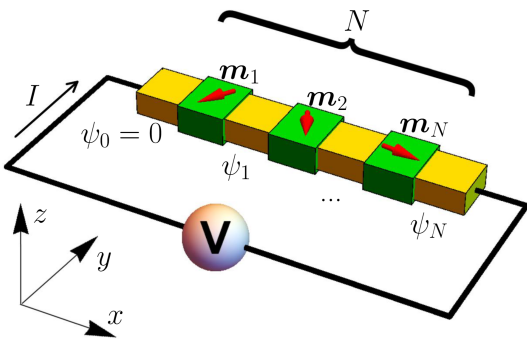


FIG. 1. Sketch of a coupled system of N φ_0 -S/F/S JJs. The dc voltage V is applied between the external leads. Magnetic moment of each JJ is shown by a red arrow. ψ_i is a phase of the superconducting region connecting i -th and $i+1$ -th weak links.

II. MODEL AND METHOD

We consider a linear chain of N coupled φ_0 - S/F/S JJs, where S means a conventional superconductor and F means a homogeneous ferromagnet characterized by a unit vector $\mathbf{m}_i = \mathbf{M}_i/|\mathbf{M}_i|$ along the direction of the magnetic moment \mathbf{M}_i of the i -th magnet in the chain, see Fig. 1. It is assumed that the ferromagnets are easy-axis magnets with the easy-axis along the z -direction. The CPR of an individual S/F/S JJ takes the form $I = I_{c,i} \sin(\varphi_i - \varphi_{0,i})$, where $I_{c,i}$ is the critical current of i -th JJ, $\varphi_i = \psi_i - \psi_{i-1}$ is the superconducting phase difference at this JJ and $\varphi_{0,i}$ is the anomalous phase shift for a given JJ. Here we consider Rashba type SOC because it arises due to the structural inversion asymmetry and is the most common type of SOC for low-dimensional ferromagnets and thin-film ferromagnet/normal metal (F/N) hybrid structures. In this case the anomalous phase shift takes the form

$$\varphi_{0,i} = r_i \hat{\mathbf{j}} \cdot (\mathbf{n} \times \mathbf{m}_i), \quad (1)$$

where $\hat{\mathbf{j}}$ is the unit vector along the Josephson current and \mathbf{n} is the unit vector describing the direction of the structural asymmetry in the system. For the case under consideration it is along the z -axis. r_i is a constant quantifying the strength of the coupling between the magnetic moment and the condensate. It depends on the material parameters of the ferromagnet, Rashba constant, length of the ferromagnetic interlayer and was calculated in the framework of different models, including ballistic Rashba ferromagnets, diffusive Rashba ferromagnets and S/F/S JJs on top of the 3D TI [26, 44–46]. The results presented below depend only on the symmetry of Eq. (1) expressing how the anomalous phase shift depends on the direction of the magnetization \mathbf{m}_i . If we choose x -axis along the Josephson current, then symmetry of our system dictates that

$$\varphi_{0,i} = r_i m_{yi}. \quad (2)$$

In the framework of our model we assume that the critical current $I_{c,i}$ does not depend on \mathbf{m}_i . In fact, the behavior of the critical current depends on the particular type of the considered S/F/S JJ. It can be independent on the magnetization direction, as it has been reported for the ferromagnets with SOC [44], or it can depend strongly on the x -component of the magnetization, as it takes place for the ferromagnetic interlayers on top of the 3D TI [26, 46]. The influence of this dependence on the behavior of the voltage-driven φ_0 -S/F/S chain is a prospect for future work.

The voltage-driven dynamics of the system can be calculated on the basis of two coupled equations. The dynamics of magnetic moments \mathbf{m}_i is described by the Landau-Lifshitz-Gilbert (LLG) equation:

$$\frac{d\mathbf{m}_i}{dt} = -\gamma \mathbf{m}_i \times \mathbf{H}_M^i + \alpha_i \mathbf{m}_i \times \frac{\partial \mathbf{m}_i}{\partial t} - \frac{\gamma r_i I(t)}{2eMV_F} [\mathbf{m}_i \times \mathbf{e}_y], \quad (3)$$

where γ is the gyromagnetic ratio, \mathbf{H}_M^i is the local effective field in the ferromagnet induced by the easy-axis magnetic anisotropy. For simplicity all the JJs are assumed to be the same, that is $\mathbf{H}_M^i \equiv (K/M)\mathbf{e}_z$, where K is the anisotropy constant, M is a magnetization of a magnet and V_F is its volume, thus $E_M^0 = KV_F/2$ is the anisotropy energy of the magnet. Contributions to \mathbf{H}_M^i resulting from the dipole-dipole interactions with other magnets in the chain can be safely disregarded because the phase-mediated interaction between the magnets is very long-range and does not decay even at submillimeter scales [41]. For typical parameters of the JJs with 3D topological insulator/ferromagnetic insulator interlayers [47, 48] at such distances between the magnets the energy of the dipole-dipole interaction should be several orders of magnitude smaller than the Josephson energy, which accounts for the phase-mediated interaction. $\alpha_i = \alpha$ is the Gilbert damping constant, $r_i = r$ and $I_{c,i} = I_c$. Relatively weak inhomogeneity of JJs parameters does not lead to qualitative changes in the results, see Appendix D. The last term in Eq. (3) describes the spin-orbit torque, exerted on the magnet by the electric current $I(t)$ [29, 41, 49–51]. The total current flowing through each of the JJs can be calculated in the framework of the RSJ-model and consists of the supercurrent and the normal quasiparticle current contributions. In the presence of magnetization dynamics the both contributions depend on the magnetization \mathbf{m}_i via the anomalous phase shift [27]:

$$I(t) = I_c \sin(\varphi_i - \varphi_{0,i}) + \frac{\hbar}{2eR_N} \frac{d(\varphi_i - \varphi_{0,i})}{dt}, \quad (4)$$

where R_N is the normal state resistance of a separate S/F/S JJ. Here we have in mind metallic weak links and disregard the capacitance of the JJs. With the condition of a dc applied voltage V , which gives $\psi_N = 2eVt/\hbar$, Eqs. (3) and (4) allow for determination of all the dynamical quantities describing the behavior of the system:

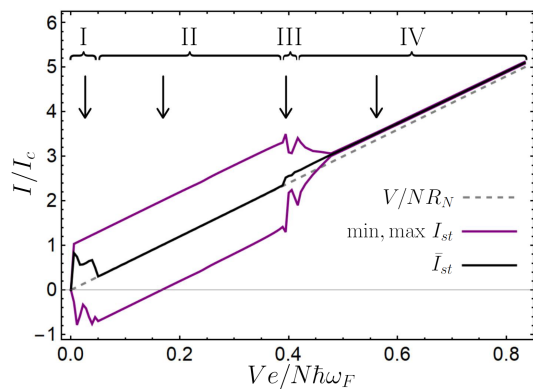


FIG. 2. IV-characteristics (solid black line) of the φ_0 -S/F/S JJs chain under the applied dc voltage. Amplitude of the current oscillations is shown by purple lines. The normal Ohm's law is shown by the dashed line. Different regimes of the voltage-driven dynamics are marked by numbers I-IV. $N = 3$, $E_J^0/E_M^0 = 2/3$, $r = 0.3$, $I_c R_N e = 0.17\hbar\omega_F$, $\alpha = 0.02$. Black arrows indicate particular voltages at which the dynamics of the system is demonstrated below.

the phase differences $\varphi_i(t) = \psi_i(t) - \psi_{i-1}(t)$, the magnetic moments of all the links $\mathbf{m}_i(t)$ and the current $I(t)$. The details of the numerical procedure are described in Appendix A.

There is an important physical reason to consider the regime of applied dc voltage, and not of applied dc current. The point is that we are interested in the signatures of the *collective* behavior of the magnetic weak links, which is a result of their interaction established via the superconducting phase and controlled by the external phase difference [41]. The regime of applied current is also frequently studied, but in relation to the system under consideration according to Eq. (3) the applied current generates independent dynamics of all the JJs in the chain. Although it is also an important problem and some interesting effects including a chaotic behavior have already been predicted [52], the collective behavior of the magnets is not excited in the applied current regime.

Because we are interested in the collective behavior of the system of coupled magnets and Josephson phases; first, let us briefly recall what the collective modes of magnetic excitations induced by the phase-mediated interaction between magnets in such a system look like [42]. At $V = 0$ and, consequently, $\psi_N = 0$, the equilibrium states of all the magnets are along the easy z -axis. In Ref. 42 it was found that such a chain of coupled φ_0 -S/F/S JJs has two eigenmodes of small excitations with the frequencies:

$$\omega_a = \gamma \sqrt{\frac{K}{M} \left(\frac{K}{M} - \lambda \right)}, \quad (5)$$

$$\omega_o = \gamma \frac{K}{M}, \quad (6)$$

where $\lambda = -r^2 E_J^0 / V_F M$ with $E_J^0 = \hbar I_c / 2e$ being the amplitude of the Josephson energy of a JJ. The small corrections to the frequencies due to the Gilbert damping constant α are neglected. ω_a is an acoustic mode because it corresponds to the motion of all the magnetic moments $\delta \mathbf{m}_i(t) = (m_{xi}(t), m_{yi}(t), 0)$ with the same phase. ω_o can be interpreted as an optic frequency corresponding to $N-1$ different modes with zero total angular y -projection of the oscillation amplitude $\sum_i m_{yi}(t) = 0$. When the

equilibrium position of the magnetic moments is along the z -axis ω_o coincides with the frequency of the ferromagnetic resonance of an isolated magnet $\omega_F = \gamma(K/M)$, but in general it may be not the case [42]. At $V \neq 0$ the both frequencies depend on the external phase ψ_N [42]. Nevertheless, the general conclusion that the system possesses acoustic and optical eigenmodes remains valid and the difference $\omega_a - \omega_o$ remains approximately constant and manifests itself in the dynamics of the system, as we will see below.

III. DIFFERENT REGIMES OF VOLTAGE-DRIVEN DYNAMICS

Now we turn to the discussion of dynamical results obtained by solving Eqs. (3) and (4). We apply dc voltage V to the chain at $t = 0$ and numerically study the dynamics at $t > 0$. After establishing a stationary regime we observe a periodic behavior of the current $I_{st}(t)$ and the magnetic moments. Fig. 2 demonstrates the IV-characteristics of the system. The black line is averaged over the period of oscillations value of the current \bar{I}_{st} for a given V . The purple lines demonstrate the maximal and minimal values of $I_{st}(t)$. We observe that depending on V the chain can be in 4 essentially different regimes, which are clearly seen in the IV-characteristics and are marked by the corresponding numbers.

In low-voltage regime I the dynamics of the phase differences $\varphi_i(t)$ is determined by frequent phase slips, what results in the appearance of a typical nonmonotonic excess current at the IV-characteristics. This regime is analogous to the voltage-driven regime of superconducting nanowires[53]. It is not related to the magnetoelectric coupling between the phase and the magnetization and can be realized even in coupled chains of conventional JJs with $\varphi_0 \equiv 0$. For this reason we have moved its discussion to Appendix B.

The “regular” regime II is the most expected. The dynamics of $\varphi_i(t)$, $I_{st}(t)$ and $m_{yi}(t)$ in this regime is presented in the upper row of Fig. 3. The phase difference is distributed uniformly among all the JJs and grows linearly $\varphi_i(t) = 2eVt/N$. $I_{st}(t)$ experiences oscillations with the Josephson frequency $\omega_J = 2eV/\hbar N$. According to Eq. (3) it acts on magnetic moments like an oscillating effective field along the y -direction, thus exciting their precession with the same frequency around the equilibrium direction, which is very close to the z -axis, but is slightly inclined from that direction due to nonzero

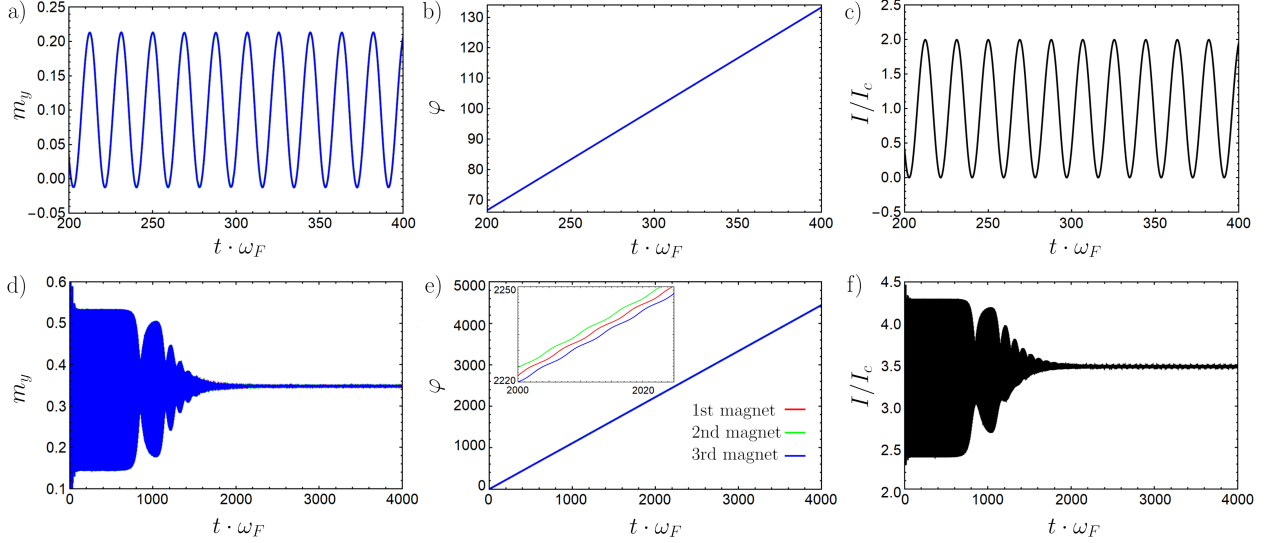


FIG. 3. Dynamics of φ_0 -S/F/S JJs chain with $N = 3$. Upper row: regime II. (a) $m_{yi}(t)$ [the same for all JJs]; (b) $\varphi_i(t)$ [the same for all JJs] and (c) $I_{st}(t)$ at $eV = 0.5\hbar\omega_F$. Only the stationary state is shown. Bottom row: regime IV. (d) $m_{yi}(t)$ [the same for all JJs]; (e) $\varphi_i(t)$, which are different for all magnets, what is shown on a larger scale in the insert. Here and below red, green and blue curves correspond to the 1st, 2nd and 3rd magnets, respectively. (f) $I(t)$ at $eV = 1.67\hbar\omega_F$. The full time range is shown including the initial and transitional regimes.

\bar{I}_{st} [24, 42].

We obtained that in the absence of the magnetoelectric coupling $\varphi_0 \equiv 0$ regime II is stable for all voltages higher the boundary of regime I. However, in the presence of the magnetoelectric coupling it appears to be unstable at voltages, which correspond to ω_J exceeding an eigenfrequency of the system. The existence of such an instability can be found analytically. To do this let us assume that $\varphi_i(t) = \omega_J t + \delta\varphi_i$ with $|\delta\varphi_i| \ll 1$. Then the electric current is $I(t) = I_c \sin(\omega_J t + \delta\varphi_i - rm_{yi}) + (1/2e/R_N)(\omega_J + \delta\dot{\varphi}_i - rm\dot{m}_{yi})$. This oscillating current acts as an exciting force on the magnets. The oscillations of the magnetic moments are also assumed to be small $m_{yi}(t) \equiv m_y(t) = m_0 + \delta m \sin(\omega_J t - rm_y - \beta)$, where β is a possible phase shift between the exciting force and the oscillations of the magnets. Up to the first order with respect to $\delta\varphi_i$ we have $I(t) = I_0(t) + \delta I(t)$ with $I_0(t) = I_c \sin(\omega_J t - rm_y) + (1/2eR_N)(\omega_J - rm\dot{m}_y)$ and $\delta I(t) = I_c \cos(\omega_J t - rm_y)\delta\varphi_i + (1/2eR_N)\delta\dot{\varphi}_i$. Due to the external condition $\psi_N = N\omega_J t$ we have $\sum_{i=1}^N \delta\varphi_i = 0$ what leads to $\delta I(t) = 0$. Linearizing this differential equation also with respect to δm we obtain:

$$\frac{\delta\dot{\varphi}_i}{2eR_N I_c} + [\cos(\omega_J t - rm_0) + r\delta m \sin(\omega_J t - rm_0 - \beta) \sin(\omega_J t - rm_0)]\delta\varphi_i = 0. \quad (7)$$

The solution of this equation takes the form:

$$\delta\varphi_i \propto e^{-\kappa t'} + \frac{2eR_N I_c}{\omega_J} \left(\frac{r\delta m \sin(2\omega_J t' - \beta)}{4} - \sin \omega_J t' \right) \quad (8)$$

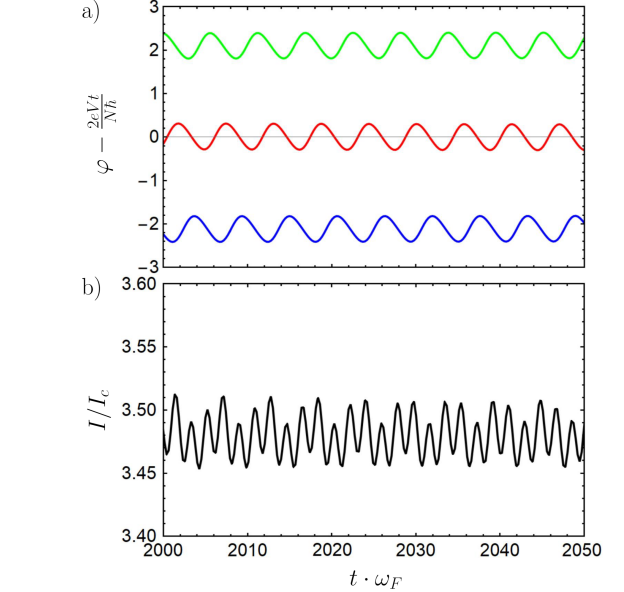


FIG. 4. Regime IV. Dynamics of (a) $\varphi_i(t)$ (with subtraction of the linear growth) and (b) $I_{st}(t)$ after establishing the steady state. $eV = 1.67\hbar\omega_F$.

where $\kappa = reR_N I_c \delta m \cos \beta$ and $t' = t - rm_0/\omega_J$. The solution $\varphi_i(t) = \omega_J t$ becomes unstable only in the presence of the magnetoelectric coupling r and when $\kappa < 0$, that is $\beta > \pi/2$, what happens if ω_J exceeds an eigenfrequency of the system.

For higher voltages, when Regime II becomes unstable

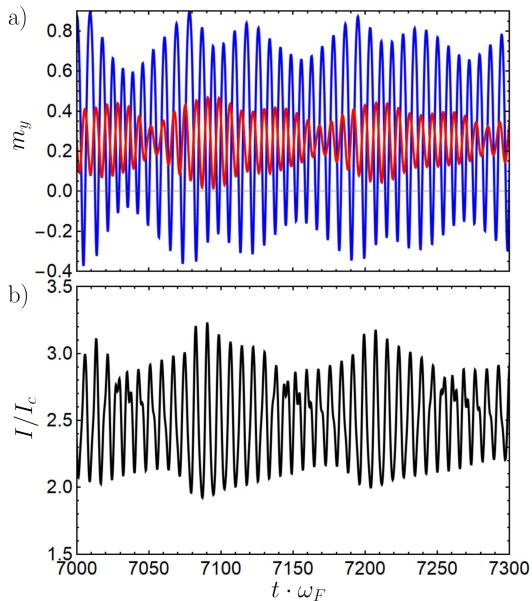


FIG. 5. Regime III. (a) Dynamics of m_{yi} . Different colors represent different magnets. The green and red curves coincide. (b) $I_{st}(t)$. Beats are seen. The carrier frequency is very close to ω_J . $eV = 1.18\hbar\omega_F$.

the system goes to another stable regimes III and IV. The dynamics of $\varphi_i(t)$, $I_{st}(t)$ and $m_{yi}(t)$ in regime IV is shown in bottom row of Fig. 3. At small t , the system behaves like in regime II, but after a quite long process of increasing phase instability and transient process, which are described in more detail in Appendix C, it goes to a new stable regime. In this regime the linear in time growth of the phase $\varphi_i(t)$ is accompanied by oscillations with the frequency ω_J with constant phase shifts between different JJs. This behavior is shown in the insert to Fig. 3(e) and in more details in Fig. 4 together with the behavior of $I_{st}(t)$. The current $I(t)$ depends on phase differences φ_i at all JJs. Due to the oscillations of the phases $\varphi_i(t)$ the frequency of $I_{st}(t)$ becomes a multiple integer of ω_J . The leading contribution to the current is given by the frequencies, which do not exceed $N\omega_J$. The amplitude of oscillations of the current and the magnetic moments becomes considerably smaller than in regime II and, simultaneously, the averaged value of the current \bar{I}_{st} increases, what is clearly seen in the IV-characteristics. It is worth noting that at $\varphi_0 = 0$ regime IV is also stable. However, we were able to numerically observe it only by turning off φ_0 at some t . If $\varphi_0 = 0$ from the very beginning, we were not able to switch the chain from regime II to regime IV.

Regime III, which is realized in a narrow voltage region

before Regime IV is even more interesting. In this voltage region ω_J is close to the eigenfrequencies of the chain. For the case under consideration ω_a and ω_o are close to each other and close to ω_F because $r^2 E_J^0 / E_M^0 \ll 1$. If this parameter would be larger the voltage-driven dynamics of the system would be more trivial because the magnetic moments quickly lie along the y -axis due to the strong magnetoelectric action of the current-induced effective field. According to estimates reported in the literature [24, 43], different regimes from $E_M/E_J \ll 1$ to $E_M/E_J > 1$ can be realized experimentally. r also can vary widely [43] from $r \ll 1$ to $r \sim 10$. Due to the proximity of the eigenfrequencies to ω_J in regime III the amplitudes of oscillations of \mathbf{m}_i are large and frequent events of the magnetization reversals \mathbf{m}_i along $\mathbf{e}_z \rightarrow -\mathbf{e}_z$ occur. Then the applied dc voltage is able to excite not only acoustic, but also the optic eigenmode. It is seen in Fig. 5(a), where the y -components of different magnetic moments m_{yi} oscillate with different amplitudes, what indicates that a superposition of the acoustic and optic modes is excited.

The current $I_{st}(t)$ in regime III, shown in Fig. 5(b) manifests beats, which are a result of oscillations with close frequencies ω_a and ω_o . The same beats are seen in the dynamics of the magnetic moments. Please note that in this regime the frequency of the oscillations of $I_{st}(t)$, $m_{yi}(t)$ and $\varphi_i(t)$ is not strictly determined by the externally forced frequency ω_J , the system adjust the frequency of oscillations by itself. This is due to the proximity to the eigenfrequencies of the magnetic system and, consequently, strong back action of the magnetic subsystem on the superconducting phase via the anomalous phase shift. Therefore, in regime III it is possible to observe the collective magnetic eigenmodes of the coupled chain of φ_0 -S/F/S JJs in the behavior of the electric current.

IV. CONCLUSIONS

The dc voltage-driven dynamics of a coupled chain of φ_0 -S/F/S JJs is investigated. Magnetoelectric coupling between the magnetic weak links and the superconducting phase leads to an instability of the conventional phase and magnetization dynamics and to transitions to qualitatively different dynamical regimes. In particular, the collective magnetic eigenmodes of the chain can be observed as beats of the ac electric current.

ACKNOWLEDGMENTS

The work has been supported by RSF project No. 22-42-04408.

Appendix A: Numerical procedure

In this section we describe technical details of the numerical procedure. Functions to be calculated are $\mathbf{m}_i(t)$, $\varphi_i(t)$. Equations (3) and (4) of the main text can be transformed to the following form (the standard form of the initial value problem) to facilitate numerical calculations:

$$\dot{\mathbf{m}}_i = -\frac{\gamma}{1+\alpha^2}[\mathbf{m}_i \times \mathbf{H}^i] - \frac{\alpha\gamma}{1+\alpha^2}[\mathbf{m}_i \times [\mathbf{m}_i \times \mathbf{H}^i]] \quad (\text{A1})$$

$$\dot{\varphi}_i = \frac{2eR_N}{\hbar}(I(t) - I_{c,i} \sin(\varphi_i - r_i m_{iy})) + r_i \dot{m}_{iy} \quad (\text{A2})$$

where

$$\mathbf{H}^i = \mathbf{H}_M^i + \frac{r_i}{2eMV_F} I(t) \mathbf{e}_y \quad (\text{A3})$$

$$I(t) = \frac{\frac{V}{R_N} + \sum_i I_{c,i} \sin(\varphi_i - r_i m_{iy}) + \frac{r_i \gamma}{1+\alpha^2} (\mathbf{e}_y \cdot ([\mathbf{m}_i \times \mathbf{H}_M^i] + \alpha [\mathbf{m}_i \times [\mathbf{m}_i \times \mathbf{H}_M^i]]))}{N - \sum_i \frac{\gamma r_i^2}{2eMV_F(1+\alpha^2)} (\mathbf{e}_y \cdot ([\mathbf{m}_i \times \mathbf{e}_y] + \alpha [\mathbf{m}_i \times [\mathbf{m}_i \times \mathbf{e}_y]]))} \quad (\text{A4})$$

Equations (A1), (A2) are solved by the explicit second order Runge-Kutta method. Time step is $\delta t = 0.002\omega_F^{-1}$, where $\omega_F = \gamma(K/M)$ is the ferromagnetic resonance frequency. Time domain $10^4\omega_F^{-1}$ was used to be sure that all transient processes are ended.

The initial conditions are $\mathbf{m}_i = \mathbf{e}_z$, $\varphi_i = 0$ which corresponds to the equilibrium state before switching on the voltage. The voltage is switched on abruptly, but it has been verified that the result (except for the transition period at times $t \sim \omega_F^{-1}$) does not depend on the method of switching on the voltage.

To add small noise to the calculation, the following term was added to the effective field:

$$\delta \mathbf{H}^i = \frac{P_{\text{noise}}}{\sqrt{dt}} \mathbf{f}_{\text{rnd}} \quad (\text{A5})$$

where \mathbf{f}_{rnd} is random Gaussian variable with unit variance. The amplitude of noise $P_{\text{noise}} = 0.0002K/(M\sqrt{\omega_F})$ was used in our calculations.

Appendix B: Low-voltage phase-slips regime

As it was discussed in the main text, in low-voltage regime I the dynamics of the phase differences $\varphi_i(t)$ is determined by phase slips. Here by an example of a chain consisting of $N = 3$ coupled φ_0 -S/F/S JJs we provide more detailed numerical results on the dynamics of the phase and the electric current in this regime. The time dependence of the phase differences $\varphi_i(t)$ at all three JJs is shown in Fig. 6. The regular linear growth is accompanied by the phase slips $\varphi_i - \varphi_j = 2\pi n$, where n is an integer number. This condition provides the current conservation $I_i(t) = I_j(t)$. Also the condition $\sum_i \varphi_i = 2eVt/\hbar$ is fulfilled.

The physical reason for the classical phase slips is well-known [see, for example, Ref. 54] and explained in Fig. 7 by considering the adiabatic limit corresponding to small V . The Josephson energy of the system takes the form:

$$E_J = \sum_i E_J^0 (1 - \cos \tilde{\varphi}_i), \quad (\text{B1})$$

where $\tilde{\varphi}_i = \tilde{\varphi} + \delta\varphi_i$. $\sum_i \delta\varphi_i = 0$ and $\tilde{\varphi} = 2eVt/N\hbar - \varphi_0$ is the externally applied phase equally distributed between all JJs shifted by the anomalous phase shift φ_0 , which is the same for all JJs in the adiabatic approximation. The energy is shown in Fig. 7(a). It is a multi-valued function of $\tilde{\varphi}$. The unstable with respect to phase-slips parts of the energy branches are shown by dashed lines. The higher energetically unfavorable parts of the branches are partially metastable. As a result the jumps between the branches occur later their crossing points $\omega_J t = (2k+1)\pi/N$, where $k = 0, \pm 1, \dots$. Due to this fact the dependence $I(\tilde{\varphi})$ is asymmetric with respect to the horizontal axis, see Fig. 7(b)

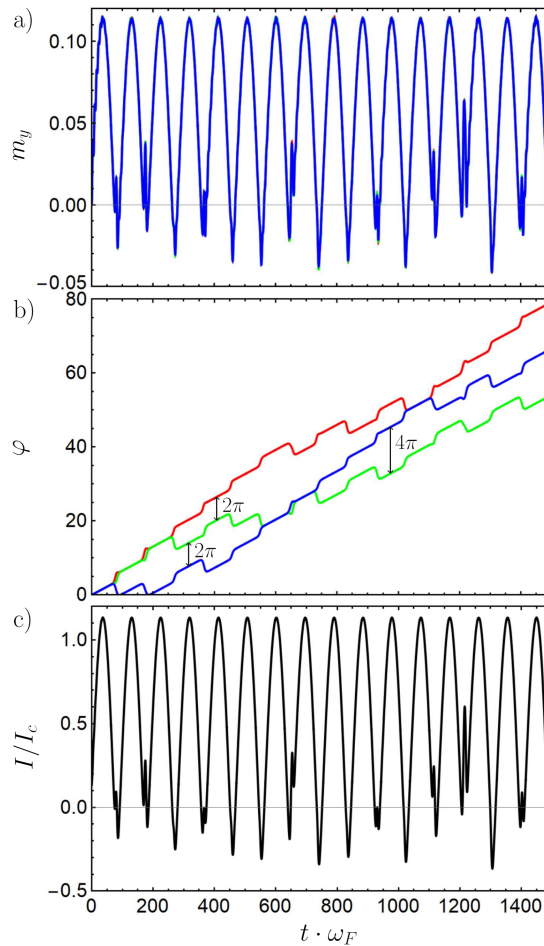


FIG. 6. Regime I. (a) $m_y(t)$ [the same at all three JJs of the chain with $N = 3$]. (b) Dynamics of the phase differences φ_i at all three JJs. (c) Oscillations of $I(t)$ with frequency ω_J . $eV = 0.067\hbar\omega_F$

($\dot{\varphi}$ is neglected in this analysis). This is the reason of the excess current with respect to the Ohm's law, which is seen in the IV-characteristics, presented in Fig. 2 of the main text.

In order to obtain numerically the results presented in Fig. 6 we assumed small noise of the magnetic moments \mathbf{m}_i . But we would like to stress that the discussed results are not related to the magnetoelectric coupling between the phase and the magnetization and can be realized even in coupled chains of conventional JJs with $\varphi_0 \equiv 0$ if we assume small fluctuations of the phases.

Appendix C: Phase instability

Here we discuss in detail the process of increasing phase instability and transition of the system to the new regime IV discussed in the main text. We apply voltage $V \neq 0$ at $t = 0$. The dynamics of the phase differences at all JJs is shown in Fig. 8 for $N = 3$. At small times all the phase differences are the same and correspond to the linear growth $\varphi_i = \omega_J t$ like in the regular regime II. However, the considered voltage exceeds the eigenfrequencies $\omega_{a,o}$ of the chain. Then we have $\kappa < 0$ in Eq. (8) of the main text and this regular growth of the phase difference becomes unstable. The process of growing instability is seen in Fig. 8(a) and in Fig. 8(b) on a larger scale. Its typical time exceeds all the characteristic time scales of the system and depends not only on the system parameters, but also on amplitude of the initial fluctuations of \mathbf{m}_i . After the system comes to the stationary state, the quantities $\varphi_i - \omega_J t$ oscillate with the same frequency ω_J , but they have different time-averaged values and there is a constant phase shift between their oscillations. We have numerically checked that the final dynamical state of the system is not unique. The phase differences always oscillate with frequency ω_J , but their time-averaged values and the phase shifts between

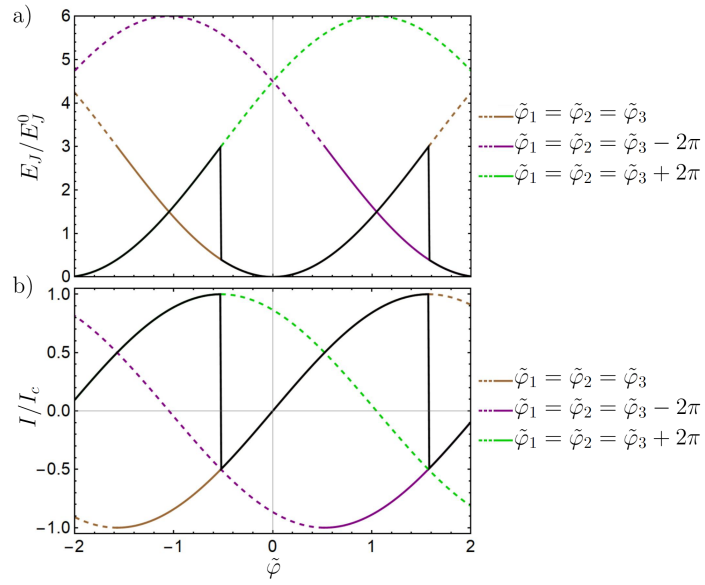


FIG. 7. (a) Josephson energy $E_J(\tilde{\varphi})$ of the coupled chain of JJs. Stable parts of the energy branches are shown by solid lines, and unstable with respect to phase slips parts are shown by dashed lines. The abrupt jumps of the black line correspond to phase slips. (b) Josephson current $I(\tilde{\varphi})$. The black lines in the both panels illustrates the dynamical variation of the chain Josephson energy and the Josephson current in the adiabatic approximation.

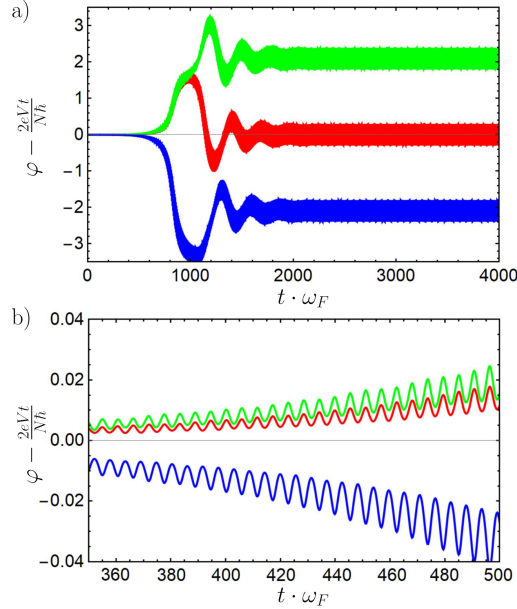


FIG. 8. Regime IV. (a) Dynamics of the phase differences φ_i at all three JJs of the chain with $N = 3$. (b) The same on a larger scale. $eV = 1.67\hbar\omega_F$.

them depend on the particular realization. Surely, all possible realizations presuppose the fulfillment of the condition $\sum \varphi_i(t) = 2eVt/\hbar$.

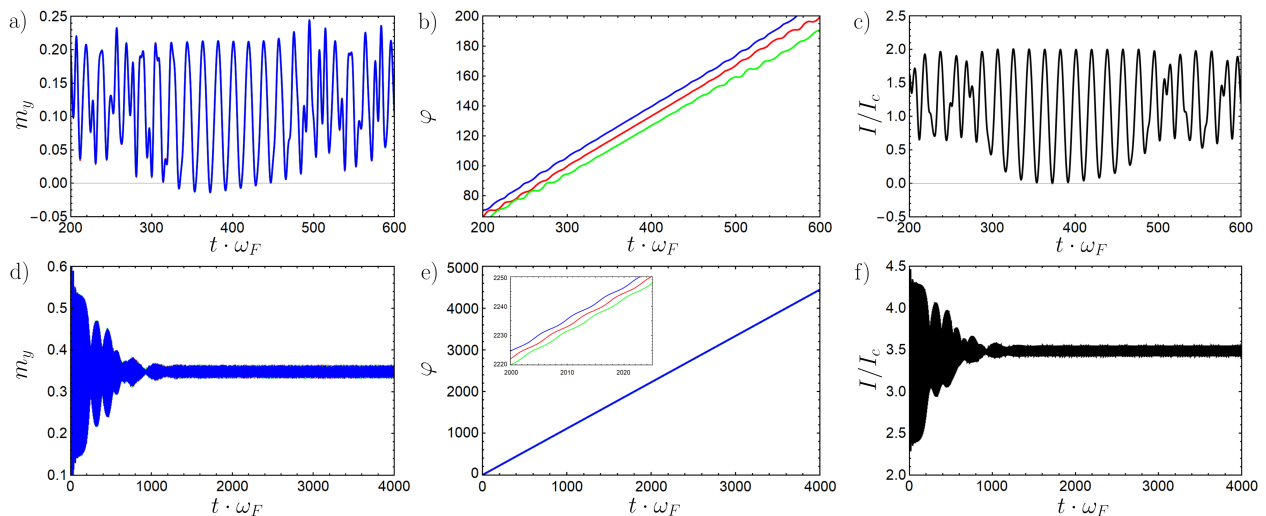


FIG. 9. Dynamics of φ_0 -S/F/S JJs chain with $N = 3$, where the critical currents of individual JJs are not the same. $\delta I_c/I_c = 2\%$. Upper row: regime II. (a) $m_{yi}(t)$ [the same for all JJs]; (b) $\varphi_i(t)$ and (c) $I_{st}(t)$ at $eV = 0.5\hbar\omega_F$. Only the stationary state is shown. Bottom row: regime IV. (d) $m_{yi}(t)$ [the same for all JJs]; (e) $\varphi_i(t)$, which are different for all magnets, what is shown on a larger scale in the insert. (f) $I(t)$ at $eV = 1.67\hbar\omega_F$. The full time range is shown including the initial and transitional regimes.

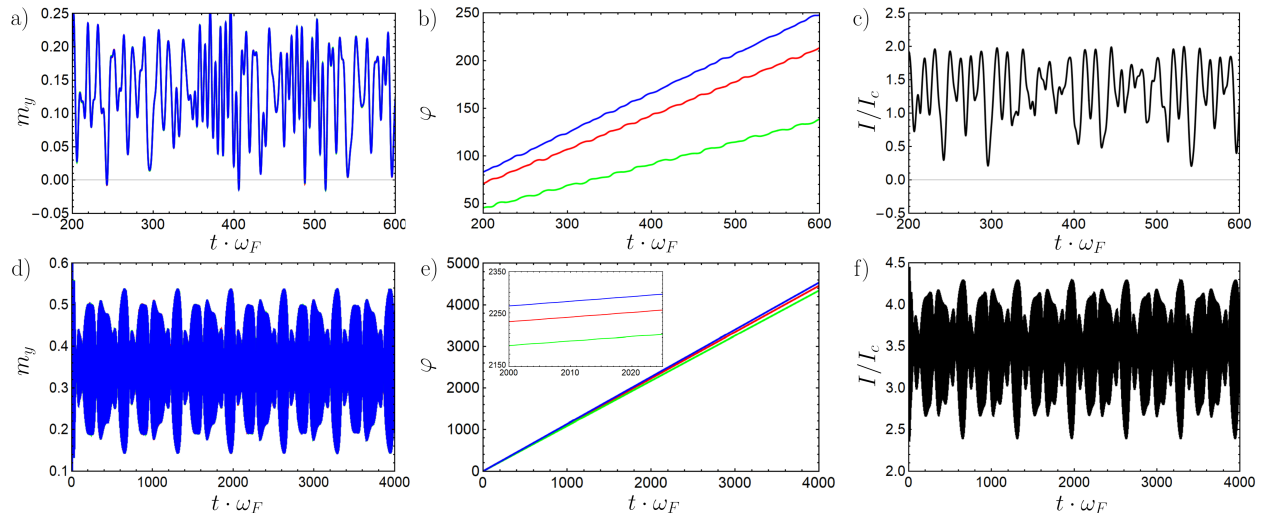


FIG. 10. The same as in Fig. 9, but for much larger variations of the critical currents $\delta I_c/I_c = 35\%$.

Appendix D: Influence of variations of individual JJs parameters

In this section we present results supporting our statement that variations of parameters of individual JJs do not prevent the system from transitioning to anomalous dynamic regimes. We assume that in the chain consisting of $N = 3$ junctions individual JJs have different critical currents I_c , $I_c \pm \delta I_c$. Figs. 9 and 10 demonstrate the results for the voltage-driven dynamics in the normal regime II (upper row) and the anomalous regime IV (bottom row). In Fig. 9 the case of small critical current variations $\delta I_c/I_c = 2\%$ is shown, while Fig. 10 corresponds to the case of much larger $\delta I_c/I_c = 35\%$. Due to the different values of the critical currents the normal regime in the both figures is characterized by different phase differences at all three JJs and, consequently, different inclines of $\varphi_i(t)$. In Fig. 10(b) it is seen more clearly than in Fig. 9(b) owing to the stronger variation of the critical currents. Because of different values $\varphi_i(t)$ the Josephson frequencies of the individual JJs are not the same. If this difference is small, it results in beats of the oscillations of $m_{yi}(t)$ and $I(t)$, see Figs. 10(a) and (c). For larger differences of the Josephson frequencies

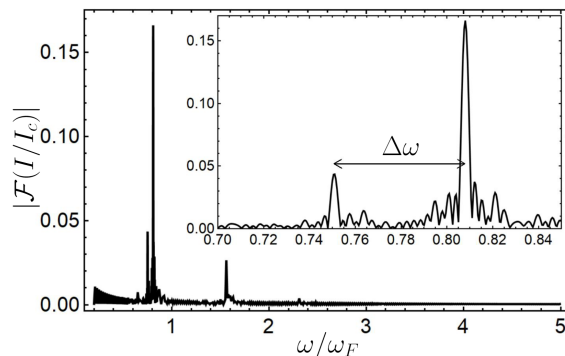


FIG. 11. Fourier transform of $I(t)$ presented in Fig. 5 of the main text. Inset: the region of the split main peak on a larger scale. $eV = 1.18\hbar\omega_F$

of individual JJs the behavior of $m_{yi}(t)$ and $I(t)$ is more complicated, see Figs. 10(d) and (f).

At the same time the anomalous regime IV is characterized by much smaller differences of the averaged incline of $\varphi_i(t)$ and smaller amplitudes of the $I(t)$ oscillations. For not very large variations of the critical currents the amplitudes of the oscillations of the magnetic moments are also suppressed in this regime. In the anomalous regime III observation of the beats corresponding to the difference of the eigenfrequencies of the chain collective modes $\omega_a - \omega_o$ is complicated by the simultaneous presence of the beats associated with the difference of the Josephson frequencies of the individual JJs.

Appendix E: Fourier analysis of current beats

Eqs. (5),(6) of the main text give us the difference between optic and acoustic mods

$$\Delta\omega = \omega_a - \omega_o = \omega_F \left(\sqrt{1 + \frac{2r^2 E_J^0}{E_M^0}} - 1 \right) \quad (\text{E1})$$

For the parameters used in Fig. 5 of the main text $\Delta\omega \approx 0.06\omega_F$. In Fig.11 the Fourier transform of beats of current is shown. The main peak is doubled (also peaks corresponding to multiple frequencies can be seen). The difference between the two frequencies that make up the beats is $0.057\omega_F$ what agrees with Eq. E1 very well.

It is important to note that since the eigenfrequencies depend on ψ_N , the frequencies ω_a, ω_o by themselves are not determined by Eqs. (5) and (6) of the main text, as it is indicated there. Nevertheless, expression for their difference Eq. E1 remains valid.

-
- [1] A. A. Golubov, M. Y. Kupriyanov, and E. Il'ichev, The current-phase relation in josephson junctions, Rev. Mod. Phys. **76**, 411 (2004).
 - [2] A. I. Buzdin, L. N. Bulaevskii, and P. S. V., Critical-current oscillations as a function of the exchange field and thickness of the ferromagnetic metal (f) in an s-f-s josephson junction, JETP Lett. **35**, 178 (1982).
 - [3] A. I. Buzdin, Proximity effects in superconductor-ferromagnet heterostructures, Rev. Mod. Phys. **77**, 935 (2005).
 - [4] V. V. Ryazanov, V. A. Oboznov, A. Y. Rusanov, A. V. Veretennikov, A. A. Golubov, and J. Aarts, Coupling of two superconductors through a ferromagnet: Evidence for a π junction, Phys. Rev. Lett. **86**, 2427 (2001).
 - [5] T. Kontos, M. Aprili, J. Lesueur, F. Genêt, B. Stephanidis, and R. Boursier, Josephson junction through a thin ferromagnetic layer: Negative coupling, Phys. Rev. Lett. **89**, 137007 (2002).
 - [6] J. Robinson, S. Piano, G. Burnell, C. Bell, and M. Blamire, Critical current oscillations in strong ferromagnetic π junctions, Physical review letters **97**, 177003 (2006).
 - [7] J. J. A. Baselmans, A. F. Morpurgo, B. J. van Wees, and T. M. Klapwijk, Reversing the direction of the supercurrent in a controllable josephson junction, Nature **397**, 43 (1999).
 - [8] T. E. Golikova, M. J. Wolf, D. Beckmann, G. A. Penzyakov, I. E. Batov, I. Bobkova, A. M. Bobkov, and

- V. V. Ryazanov, Controllable supercurrent in mesoscopic superconductor-normal metal-ferromagnetic crosslike josephson structures, *Superconductor Science and Technology* (2021).
- [9] R. R. Schulz, B. Chesca, B. Götz, C. W. Schneider, A. Schmehl, H. Bielefeldt, H. Hilgenkamp, J. Mannhart, and C. Tsuei, Design and realization of an all d-wave dc π -superconducting quantum interference device, *Applied Physics Letters* **76**, 912 (2000).
- [10] H. I. Jørgensen, T. Novotný, K. Grove-Rasmussen, K. Flensberg, and P. Lindelof, Critical current $0-\pi$ transition in designed josephson quantum dot junctions, *Nano letters* **7**, 2441 (2007).
- [11] J. A. van Dam, Y. V. Nazarov, E. P. A. M. Bakkers, S. De Franceschi, and L. P. Kouwenhoven, Supercurrent reversal in quantum dots, *Nature* **442**, 667 (2006).
- [12] C. T. Ke, C. M. Moehle, F. K. de Vries, C. Thomas, S. Metti, C. R. Guinn, R. Kallaher, M. Lodari, G. Scappucci, T. Wang, *et al.*, Ballistic superconductivity and tunable π -junctions in insb quantum wells, *Nature communications* **10**, 1 (2019).
- [13] A. K. Feofanov, V. A. Oboznov, V. V. Bol'ginov, J. Lisenfeld, S. Poletto, V. V. Ryazanov, A. N. Rossolenko, M. Khabipov, D. Balashov, A. B. Zorin, P. N. Dmitriev, V. P. Koshelets, and A. V. Ustinov, Implementation of superconductor/ferromagnet/ superconductor π -shifters in superconducting digital and quantum circuits, *Nature Physics* **6**, 593 (2010).
- [14] T. Yamashita, K. Tanikawa, S. Takahashi, and S. Maekawa, Superconducting π qubit with a ferromagnetic josephson junction, *Phys. Rev. Lett.* **95**, 097001 (2005).
- [15] A. V. Shcherbakova, K. G. Fedorov, K. V. Shulga, V. V. Ryazanov, V. V. Bolginov, V. A. Oboznov, S. V. Egorov, V. O. Shkolnikov, M. J. Wolf, D. Beckmann, and A. V. Ustinov, Fabrication and measurements of hybrid nb/al josephson junctions and flux qubits with π -shifters, *Superconductor Science and Technology* **28**, 025009 (2015).
- [16] I. V. Bobkova, A. M. Bobkov, and M. A. Silaev, Magneto-electric effects in josephson junctions, *Journal of Physics: Condensed Matter* **34**, 353001 (2022).
- [17] Y. M. Shukrinov, Anomalous josephson effect, *Physics-Uspokhi* **65**, 317 (2022).
- [18] W. Mayer, M. C. Dartiailh, J. Yuan, K. S. Wickramasinghe, E. Rossi, and J. Shabani, Gate controlled anomalous phase shift in al/inas josephson junctions, *Nature Communications* **11**, 212 (2020).
- [19] D. B. Szombati, S. Nadj-Perge, D. Car, S. R. Plissard, E. P. A. M. Bakkers, and L. P. Kouwenhoven, Josephson φ_0 -junction in nanowire quantum dots, *Nature Physics* **12**, 568 (2016).
- [20] A. Assouline, C. Feuillet-Palma, N. Bergeal, T. Zhang, A. Mottaghizadeh, A. Zimmers, E. Lhuillier, M. Eddrie, P. Atkinson, M. Aprili, and H. Aubin, Spin-orbit induced phase-shift in bi2se3 josephson junctions, *Nature Communications* **10**, 126 (2019).
- [21] A. Murani, A. Kasumov, S. Sengupta, Y. A. Kasumov, V. T. Volkov, I. I. Khodos, F. Brisset, R. Delagrè, A. Chepelianskii, R. Deblock, H. Bouchiat, and S. Guéron, Ballistic edge states in bismuth nanowires revealed by squid interferometry, *Nature Communications* **8**, 15941 (2017).
- [22] J. Linder and J. W. A. Robinson, Superconducting spintronics, *Nature Physics* **11**, 307 (2015).
- [23] M. Eschrig, Spin-polarized supercurrents for spintronics: a review of current progress, *Reports on Progress in Physics* **78**, 104501 (2015).
- [24] F. Konschelle and A. Buzdin, Magnetic moment manipulation by a josephson current, *Phys. Rev. Lett.* **102**, 017001 (2009).
- [25] Y. M. Shukrinov, I. R. Rahmonov, K. Sengupta, and A. Buzdin, Magnetization reversal by superconducting current in ϕ josephson junctions, *Applied Physics Letters* **110**, 182407 (2017).
- [26] M. Nashaat, I. V. Bobkova, A. M. Bobkov, Y. M. Shukrinov, I. R. Rahmonov, and K. Sengupta, Electrical control of magnetization in superconductor/ferromagnet/superconductor junctions on a three-dimensional topological insulator, *Phys. Rev. B* **100**, 054506 (2019).
- [27] D. S. Rabinovich, I. V. Bobkova, A. M. Bobkov, and M. A. Silaev, Resistive state of superconductor-ferromagnet-superconductor josephson junctions in the presence of moving domain walls, *Phys. Rev. Lett.* **123**, 207001 (2019).
- [28] C. Guarcello and F. Bergeret, Cryogenic memory element based on an anomalous josephson junction, *Phys. Rev. Appl.* **13**, 034012 (2020).
- [29] I. V. Bobkova, A. M. Bobkov, I. R. Rahmonov, A. A. Mazanik, K. Sengupta, and Y. M. Shukrinov, Magnetization reversal in superconductor/insulating ferromagnet/superconductor josephson junctions on a three-dimensional topological insulator, *Phys. Rev. B* **102**, 134505 (2020).
- [30] M. Gibertini, M. Koperski, A. F. Morpurgo, and K. S. Novoselov, Magnetic 2d materials and heterostructures, *Nature Nanotechnology* **14**, 408 (2019).
- [31] L. Ai, E. Zhang, J. Yang, X. Xie, Y. Yang, Z. Jia, Y. Zhang, S. Liu, Z. Li, P. Leng, X. Cao, X. Sun, T. Zhang, X. Kou, Z. Han, F. Xiu, and S. Dong, Van der waals ferromagnetic josephson junctions, *Nature Communications* **12**, 6580 (2021).
- [32] K. Kang, H. Berger, K. Watanabe, T. Taniguchi, L. Forró, J. Shan, and K. F. Mak, van der waals π josephson junctions, *Nano Letters* **22**, 5510 (2022).
- [33] C.-Z. Chang, J. Zhang, M. Liu, Z. Zhang, X. Feng, K. Li, L.-L. Wang, X. Chen, X. Dai, Z. Fang, X.-L. Qi, S.-C. Zhang, Y. Wang, K. He, X.-C. Ma, and Q.-K. Xue, Thin films of magnetically doped topological insulator with carrier-independent long-range ferromagnetic order, *Advanced Materials* **25**, 1065 (2013).
- [34] X. Kou, M. Lang, Y. Fan, Y. Jiang, T. Nie, J. Zhang, W. Jiang, Y. Wang, Y. Yao, L. He, and K. L. Wang, Interplay between different magnetisms in cr-doped topological insulators, *ACS Nano* **7**, 9205 (2013).
- [35] X. Kou, L. He, M. Lang, Y. Fan, K. Wong, Y. Jiang, T. Nie, W. Jiang, P. Upadhyaya, Z. Xing, Y. Wang, F. Xiu, R. N. Schwartz, and K. L. Wang, Manipulating surface-related ferromagnetism in modulation-doped topological insulators, *Nano Letters* **13**, 4587 (2013).
- [36] C.-Z. Chang, W. Zhao, D. Y. Kim, H. Zhang, B. A. As-saf, D. Heiman, S.-C. Zhang, C. Liu, M. H. W. Chan, and J. S. Moodera, High-precision realization of robust quantum anomalous hall state in a hard ferromagnetic topological insulator, *Nature Materials* **14**, 473 (2015).
- [37] Z. Jiang, F. Katmis, C. Tang, P. Wei, J. S. Moodera, and J. Shi, A comparative transport study of bi2se3 and bi2se3/yttrium iron garnet, *Applied Physics Letters* **104**,

- 222409 (2014).
- [38] P. Wei, F. Katmis, B. A. Assaf, H. Steinberg, P. Jarillo-Herrero, D. Heiman, and J. S. Moodera, Exchange-coupling-induced symmetry breaking in topological insulators, *Phys. Rev. Lett.* **110**, 186807 (2013).
- [39] Z. Jiang, C.-Z. Chang, C. Tang, P. Wei, J. S. Moodera, and J. Shi, Independent tuning of electronic properties and induced ferromagnetism in topological insulators with heterostructure approach, *Nano Letters* **15**, 5835 (2015).
- [40] Z. Jiang, C.-Z. Chang, C. Tang, J.-G. Zheng, J. S. Moodera, and J. Shi, Structural and proximity-induced ferromagnetic properties of topological insulator-magnetic insulator heterostructures, *AIP Advances* **6**, 055809 (2016).
- [41] G. A. Bobkov, I. V. Bobkova, and A. M. Bobkov, Long-range interaction of magnetic moments in a coupled system of superconductor-ferromagnet-superconductor josephson junctions with anomalous ground-state phase shift, *Phys. Rev. B* **105**, 024513 (2022).
- [42] G. A. Bobkov, I. V. Bobkova, and A. M. Bobkov, Magnetic eigenmodes in chains of coupled φ_0 -josephson junctions with ferromagnetic weak links, *JETP Lett.* (2024).
- [43] G. A. Bobkov, I. V. Bobkova, and A. M. Bobkov, Controllable magnetic states in chains of coupled φ_0 josephson junctions with ferromagnetic weak links, *Phys. Rev. B* **109**, 054523 (2024).
- [44] A. Buzdin, Direct coupling between magnetism and superconducting current in the josephson φ_0 junction, *Phys. Rev. Lett.* **101**, 107005 (2008).
- [45] Bergeret, F. S. and Tokatly, I. V., Theory of diffusive josephson junctions in the presence of spin-orbit coupling, *EPL* **110**, 57005 (2015).
- [46] A. Zyuzin, M. Alidoust, and D. Loss, Josephson junction through a disordered topological insulator with helical magnetization, *Phys. Rev. B* **93**, 214502 (2016).
- [47] M. Veldhorst, M. Snelder, M. Hoek, T. Gang, V. K. Guduru, X. L. Wang, U. Zeitler, W. G. van der Wiel, A. A. Golubov, H. Hilgenkamp, and A. Brinkman, Josephson supercurrent through a topological insulator surface state, *Nature Materials* **11**, 417 (2012).
- [48] J. Xiao, G. E. W. Bauer, K.-c. Uchida, E. Saitoh, and S. Maekawa, Theory of magnon-driven spin seebeck effect, *Phys. Rev. B* **81**, 214418 (2010).
- [49] T. Yokoyama, Current-induced magnetization reversal on the surface of a topological insulator, *Phys. Rev. B* **84**, 113407 (2011).
- [50] I. Mihai Miron, G. Gaudin, S. Auffret, B. Rodmacq, A. Schuhl, S. Pizzini, J. Vogel, and P. Gambardella, Current-driven spin torque induced by the rashba effect in a ferromagnetic metal layer, *Nature Materials* **9**, 230 (2010).
- [51] I. V. Bobkova, A. M. Bobkov, and M. A. Silaev, Spin torques and magnetic texture dynamics driven by the supercurrent in superconductor/ferromagnet structures, *Phys. Rev. B* **98**, 014521 (2018).
- [52] A. A. Mazanik, A. E. Botha, I. R. Rahmonov, and Y. M. Shukrinov, Hysteresis and chaos in anomalous josephson junctions without capacitance (2023), arXiv:2311.00597 [cond-mat.supr-con].
- [53] D. Y. Vodolazov, F. M. Peeters, L. Piraux, S. Mátéfi-Tempfli, and S. Michotte, Current-voltage characteristics of quasi-one-dimensional superconductors: An *s*-shaped curve in the constant voltage regime, *Phys. Rev. Lett.* **91**, 157001 (2003).
- [54] I. M. Pop, I. Protopopov, F. Lecocq, Z. Peng, B. Panetier, O. Buisson, and W. Guichard, Measurement of the effect of quantum phase slips in a josephson junction chain, *Nature Physics* **6**, 589 (2010).